Submitted to

32nd International Conference on High Energy Physics, ICHEP04, August 16, 2004, Beijing

Abstract: **5-0760**

Parallel Session **5**

www-h1.desy.de/h1/www/publications/conf/conf_list.html

Measurement of Beauty Photoproduction at HERA Using Inclusive Lifetime Tagging

H1 Collaboration

Abstract

A measurement of the beauty photoproduction cross section at the ep collider HERA is presented. The data were collected in the years 1999 and 2000 and correspond to an integrated luminosity of 57.7pb^{-1}. Events are selected with two or more jets with large transverse momentum, $p_t^{jet_{1(2)}} > 11(8)$ GeV, in the central rapidity range, $-0.88 < \eta^{jet} < 1.3$. The lifetime signature of b-flavoured hadrons is exploited to determine the fraction of events in the sample containing beauty. Differential cross sections as a function of the jet transverse momentum, the rapidity and x_γ^{obs} are measured in the photoproduction region $Q^2 < 1$ GeV^2, with inelasticity $0.15 < y < 0.8$. The results are compared with calculations in next-to-leading order perturbative QCD and Monte Carlo models as implemented in PYTHIA and CASCADE.

1 Introduction

A measurement of differential beauty photoproduction cross sections in ep collisions at HERA is presented here. The analysis covers the photoproduction region, where the virtuality of the photon emitted from the incoming positron is small, $Q^2 \sim 0$. In this process, the production of beauty quarks is expected to be dominated by photon-gluon fusion, $\gamma g \rightarrow b\bar{b}$, where the photon interacts with a gluon from the proton to produce heavy quarks in the final state. The measurement is compared to calculations in perturbative QCD (pQCD) at next-to-leading order (NLO) in which the mass m_b of the b-quark provides a hard scale.

For the measurement presented here, a similar analysis technique is used as in a recent H1 measurement in deep inelastic scattering (DIS) at $Q^2 > 110$ GeV^2 [1]. The beauty cross section is determined using a fit to the lifetime signature of charged particles in jets. This inclusive method yields measurements of differential cross sections that extend to larger values of transverse momenta than in previous HERA analyses in which leptons from beauty quark decays were used to measure beauty cross sections [2, 3, 4, 5, 6, 7].

Events with two jets in the final state are selected to measure the beauty photoproduction cross section

$$\sigma(e^+p \rightarrow e^+b\bar{b}X \rightarrow e^+ + jj + X').$$

The cross section is measured differentially as a function of the transverse momentum and pseudo-rapidity of the leading jet and of x_γ^{obs}, defined as the fraction of the $(E - p_z)$ of the hadronic system that is carried by the two highest p_T jets:

$$x_\gamma^{obs} = \frac{(E-p_z)_{jet_1} + (E-p_z)_{jet_2}}{(E-p_z)_h}.$$

In LO QCD, x_γ^{obs} is the fraction of the photon's energy that enters the hard interaction.

2 Detector Description

The H1 detector is described in detail in [8]. Charged particles emerging from the interaction region are measured by the central tracking detector (CTD) in the pseudo-rapidity range $-1.74 < \eta < 1.74$[1]. The CTD consists of two large cylindrical central jet drift chambers (CJCs), two z-chambers and two multi-wire proportional chambers arranged concentrically around the beam-line within a solenoidal magnetic field of 1.15 T. The CTD provides triggering information based on track segments in the r-ϕ plane from the CJC and the z-position of the vertex from the multi-wire proportional chambers.

The CJC tracks are linked with hits in the Central Silicon Tracking detector (CST) [9], which consists of two cylindrical layers of silicon strip sensors, surrounding the beam pipe at radii of $R = 57.5$ mm and $R = 97$ mm from the beam axis. These double-sided sensors, with readout strip pitches of 50 μm and 88 μm, provide resolutions of 12 μm in r-ϕ and 25 μm in z. Average

[1]The pseudo-rapidity η of an object with polar angle θ is given by $\eta = -\ln\ \tan(\theta/2)$, where θ is measured with respect to the z-axis given by the proton beam direction.

hit efficiencies are 97 (92)% in r-ϕ (z). For the measurement of the impact parameter, tracks are used with two hits in the CST r-ϕ-layers. For these tracks the measurement of the transverse distance of closest approach has a resolution of $\sigma_{DCA} \approx 33\ \mu\text{m} \oplus 90\ \mu\text{m}/p_T[\text{GeV}]$. The first term represents the intrinsic resolution and includes the uncertainty of the CST alignment, the second gives the contribution from multiple scattering in the beam pipe.

The energies of final state particles are determined using CTD track information and measurements of the energy deposited in the liquid argon (LAr) calorimeter, which surrounds the tracking chambers and covers the range $-1.5 < \eta < 3.4$. The backward region ($-4.0 < \eta < -1.4$) is covered by a lead–scintillating fibre calorimeter (SPACAL [10]) with electromagnetic and hadronic sections. The calorimeters are surrounded by the iron return yoke of the solenoidal magnet.

3 Data Selection and Monte Carlo Samples

The data used in this analysis were recorded in 1999 and 2000 and correspond to an integrated luminosity of $57.7\,\text{pb}^{-1}$. The events were triggered by a combination of signals from the calorimeter, the central drift chambers and the multi-wire proportional chambers. Photoproduction events are selected by requiring that there be no high energy electromagnetic cluster anywhere in the calorimeter. This restricts the range of negative four-momentum transfer squared to $Q^2 < 1\ \text{GeV}^2$. Background from remaining DIS events in which the scattered electron simulates a jet, is removed by requiring that the transverse jet size $R > 0.02$ and $m^{jet}/p_t^{jet} > 0.1$ where m^{jet} is the reconstructed mass, calculated from the jet daughter particles, and p_t^{jet} the transverse momentum of the jet. The inelasticity y is calculated using the Jacquet-Blondel method [11], and the measurement is made in the range $0.15 < y < 0.8$. Jets are reconstructed using the inclusive k_t algorithm [12] with radius $R = 1$ in the η-ϕ plane. The p_T-recombination scheme is applied giving massless jets. The selection requires that there be at least two jets in the central rapidity range $-0.88 < \eta < 1.3$ with transverse energy ${p_t^{jet}}_{1(2)} > 11(8)$ GeV.

Monte Carlo event samples for the processes $ep \to eb\bar{b}X$, $ep \to ec\bar{c}X$ and light quark production are generated using the PYTHIA program [13] which is based on leading order QCD and uses parton showers to simulate higher order effects. PYTHIA simulates direct and resolved photon processes and also includes excitation processes, in which one heavy quark (c or b) originates from the resolved photon or the proton. PYTHIA is run in an inclusive mode and generates all the above processes using massless matrix elements. The CTEQ5L [14] parton densities are used for the proton and those of GRVG-LO [15] for the photon. For the fragmentation of charm and beauty quarks, the Peterson function [16] is used.

4 NLO QCD Calculation

Calculations in perturbative QCD are performed to next-to-leading order using the program FMNR by Frixione *et al.* [17] which implements the cross section calculation in a fixed order massive scheme, i.e. the b-quarks are generated exclusively in the hard process via boson–gluon

fusion diagrams, assuming the proton and photon to contain only light quarks. The calculations are performed in the DIS scheme using a value of 4.75 GeV for the b-quark mass and the CTEQ5D parton distributions [14] for the proton. The renormalisation and factorisation scales, μ_r and μ_f, are set to the transverse mass $m_t = \sqrt{m_b^2 + (p_t^b)^2}$. The GRV-G HO distribution [15] is used for the resolved photon.

FMNR provides parton level event distributions, i.e. two or three outgoing partons, a b-quark, a $\bar{b}$-quark and possibly a gluon. Parton level jets are reconstructed using the inclusive k_t jet-algorithm in the p_t recombination scheme. To allow comparisons with the data, corrections to the hadron level are determined using the PYTHIA Monte Carlo event generator. At the hadron level, jets are constructed using the inclusive k_t algorithm [12] using all generated stable particles including neutrinos. The parton to hadron level corrections are found to be less than 5% in all bins except for the region $0.7 < x_\gamma^{obs} < 0.85$ ($0.85 < x_\gamma^{obs} < 1$) where the correction is $\sim 40\%$ ($\sim 15\%$).

The theoretical uncertainties of the NLO calculation have been estimated by variation of the renormalisation and factorisation scale parameters up and down by a factor of two (in the same direction, i.e. $\mu_R = \mu_f$) and the b-mass between 4.5 and 5 GeV. These variations, added linearly, lead to a change in the cross section predictions of 20–30%. The cross section variation when using other proton structure functions such as MRSG or MRST1 [18] is less than 8% in all regions of the measurement. The latter uncertainty is added to the scale uncertainties in quadrature.

5 Lifetime Tag Observables

The analysis is based on CTD tracks which are linked to hits in both r-ϕ layers of the CST in order to improve the precision of the track parameters. In this paper, CST-improved CTD tracks are referred to as "CST tracks". CST tracks are required to have a minimum transverse momentum of 500 MeV and a polar angle $30^\circ < \Theta_{track} < 150^\circ$. CST tracks are associated to the jet axis of one of the two highest p_t jets if they lie within a cone of 1 in η-ϕ space centred about the jet axis. For the final sample, only those events are selected in which at least one associated CST track is found.

The transverse momentum $p_t^{jet_1}$ and the pseudo-rapidity η^{jet_1} distribution of the leading jet, i.e. that with highest p_t, are shown in figure 1a and b. Figure 1c shows x_γ^{obs} reconstructed from both jets. The data are compared to the Monte Carlo simulation PYTHIA (see section 3) which gives a good description of the data. The transverse momentum and polar angle distributions of CST tracks are compared to the Monte Carlo simulation in figure 2a and b. The number of CST tracks in the two leading jets is shown in figure 2c. The simulation also gives a reasonable description of these distributions.

The primary event vertex is reconstructed from all tracks (with or without CST hits) taking into account the position and spread of the beam interaction region. The transverse extensions of the beam interaction region are measured to be $145\ \mu\mathrm{m}$ in x and $25\ \mu\mathrm{m}$ in y for the data-taking period considered here. The mean position of the beam is measured as the average over many events; the resulting error on the mean position is small in comparison to the size of the beam-spot, with a typical uncertainty of $\sim 5\ \mu\mathrm{m}$.

In this analysis, the signed track impact parameter with respect to the event vertex is used to separate the different quark flavours. The signed impact parameter is defined as positive if the angle between the jet axis and the line between the vertex and distance of closest approach of the track to the vertex is less than 90°, and is defined as negative otherwise. The impact parameter distribution (figure 3a) is seen to be asymmetric; the number of positive values exceeds the number of negative values, indicating the presence of long lived particles. The simulation gives a reasonable description of the data. The component of the simulation that arises from light quarks is almost symmetric at small distance of closest approach (DCA). The c component has a moderate asymmetry and the b component shows a marked asymmetry with an exponential fall-off to positive values of DCA. The asymmetry seen at $|\mathrm{DCA}| > 0.1$ cm is mainly due to long lived strange particles such as K^0_S. In order to reduce the effects of the strange component, a cut of $|\mathrm{DCA}| < 0.1$ cm is imposed. The significance [19], defined as the ratio of the DCA to its error, is shown in figure 3b for all CST tracks with $|\mathrm{DCA}| < 0.1$ cm. Apart from the tails the simulation provides a good description of the data.

The separation of charm and beauty events is further enhanced by using different significance distributions for events with different track multiplicities. The first significance distribution S_1 is defined for events where exactly one CST track is found in at least one of the leading two jets, and is simply the significance of this track. The second significance distribution S_2 is defined for events with two or more CST tracks associated to at least one of these jets and is the significance of the track with the second highest absolute significance. Events in which the tracks with the first and second highest absolute significance in a jet have different signs are removed from the S_2 distribution. This latter condition removes around 50% of events from the S_2 distribution, predominantly from the light quark event sample. The S_1 and S_2 distributions are shown in figure 4.

In order to substantially reduce the uncertainty due to the DCA resolution and the light quark normalisation, the negative bins in the S_1 and S_2 distributions are subtracted from the positive. The subtracted distributions are shown in figure 5. The resulting distributions are dominated by c quark events[2], with an increasing b fraction towards increasing significance. The contribution from light quarks is seen to be small.

6 Determination of the Beauty Component

The b, c and light quark fractions in the data are extracted by simultaneously fitting the subtracted S_1 and S_2 distributions N_i^{data} and the total number of events N_{tot}^{data} with the Monte Carlo b, c and light quark distributions used as templates in each interval of the measurement. The Monte Carlo b, c and light quark distributions are allowed to be modified by the scale factors P_b, P_c and P_l, respectively, such that

$$\begin{aligned}\chi^2 &= \sum_i \frac{(N_i^{\mathrm{data}} - P_b N_{bi}^{\mathrm{MC}} - P_c N_{ci}^{\mathrm{MC}} - P_l N_{li}^{\mathrm{MC}})^2}{\sigma^2(N_i^{\mathrm{data}}) + (P_b\sigma(N_{bi}^{\mathrm{MC}}))^2 + (P_c\sigma(N_{ci}^{\mathrm{MC}}))^2 + (P_l\sigma(N_{li}^{\mathrm{MC}}))^2} \\ &+ \frac{(N_{\mathrm{tot}}^{\mathrm{data}} - P_b N_{\mathrm{tot}b}^{\mathrm{MC}} - P_c N_{\mathrm{tot}c}^{\mathrm{MC}} - P_l N_{\mathrm{tot}l}^{\mathrm{MC}})^2}{\sigma^2(N_{\mathrm{tot}}^{\mathrm{data}}) + (P_b\sigma(N_{\mathrm{tot}b}^{\mathrm{MC}}))^2 + (P_c\sigma(N_{\mathrm{tot}c}^{\mathrm{MC}}))^2 + (P_l\sigma(N_{\mathrm{tot}l}^{\mathrm{MC}}))^2}\end{aligned} \quad (1)$$

[2]Events that contain c hadrons resulting from the decay of b hadrons are not included in the definition of c quark events.

is minimized, where i runs over all bins of S_1 and S_2 with significances < 10.

The results of the fit to the complete data sample are shown in figure 5. The fit gives acceptable χ^2 values for the total event sample and for all bins of the measurement. Consistent results are also found when fitting different significance distributions, for example fitting the unsubtracted S_1 or S_2 distributions either simultaneously or alone, and when fitting the significance distributions varying the cut on the DCA. Consistent results in all bins are also obtained when using the multi-impact parameter probability observable as described below (section 7).

The total systematic error on the beauty cross section is estimated to be 21%. The dominant contributions are the uncertainties in the description of the track resolution and the track efficiency, leading to errors on the cross section of $\sim 10\%$ each. Model dependent uncertainties, such as the uncertainties on the various D and B meson lifetimes, decay branching fractions and mean charge multiplicites are estimated to contribute 7% to the total systematic uncertainty.

7 Measurement Using a Multi-Impact Parameter Probability

The results are cross checked using an alternative method to separate the quark flavours also based on the use of the significance distributions of the selected tracks S_i. The method was employed by the ALEPH collaboration [19].

The quantity

$$P(S_i) = \frac{1}{\sqrt{2\pi}} \int_{\chi^2}^{\infty} e^{-t^2} dt,$$

where $\chi_i^2 = S_i^2$, can be interpreted as the probability that a track originates at the primary vertex. The probability for tracks with negative significance is set to unity. A multi impact parameter (MIP) probability P_{MIP} is then constructed by combining the probabilities of the N CST tracks within each jet:

$$P_{MIP} = \Pi \sum_{j=0}^{N-1} (-\ln \Pi)^j / j!,$$

where j runs over all CST tracks and

$$\Pi = \prod_{i=1}^{N} P(S_i)$$

The distribution of the negative logarithm $-\log(P_{MIP})$ for both jets is shown in figure 6. The contributions made by b, c and uds to the data are obtained by fitting [20, 21] the measured $-\log(P_{MIP})$ distribution using the Monte Carlo expectations for the shapes of each of these quark flavours. The fraction of b-events obtained from a fit to the MIP probability, when converted into a cross section, is found to agree with the result obtained by the method described above (section 6).

8 Results

The fit results are converted to a measurement of the beauty cross section by determining the scale factor P_b from the fit according to equation 1 for the samples in each bin. The cross section results are then obtained by multiplying the cross sections predicted by the Monte Carlo simulation by P_b. The total dijet beauty photoproduction cross section in the range $Q^2 < 1$ GeV^2, $0.15 < y < 0.8$, $p_t^{jet_{1,2}} > 11(8)$ GeV and $-0.88 < \eta^{jet_{1,2}} < 1.3$ is measured to be

$$\sigma(ep \to eb\bar{b}X \to ejjX) = 145 \pm 18(stat.) \pm 30(sys.)\text{pb}.$$

Figures 7–9 show the measured differential cross sections as a function of $p_t^{jet_1}$, η^{jet_1} and x_γ^{obs}, respectively. The data are compared with predictions from the NLO QCD calculation FMNR as well as from the Monte Carlo programs PYTHIA and CASCADE [22]. The latter implements the CCFM [23] evolution equation using off-shell matrix elements convoluted with k_t-unintegrated parton distributions in the proton.

The data are found to be higher than the prediction from the NLO QCD calculation. While both data and theory errors are large, the main difference between the data and the NLO calculation appears to originate in the region of positive values of rapidity, as can be seen in figure 8, and small values of x_γ^{obs}, where the prediction lies significantly below the data. In these regions the contribution to the cross section from events with resolved photons is particularly large. The prediction from PYTHIA for this contribution is indicated in the figures 7–8 by the dashed-dotted line.

PYTHIA and CASCADE give a good description of the shapes of the data distributions. However, the data are generally higher in normalisation than the PYTHIA (CASCADE) prediction by a factor ~ 1.8 (~ 1.6).

9 Conclusions

A measurement of the beauty dijet photoproduction cross section at HERA has been presented. The measurement makes use of the precise tracking information available from the H1 vertex detector. The b cross section is determined by making use of the b lifetime distribution. Two different lifetime tag techniques have been used. The differential cross sections, measured as a function of transverse momentum of the leading jet $d\sigma/dp_t^{jet_1}$, the rapidity of the jet η^{jet_1} and x_γ^{obs} are found to be higher than a calculation in perturbative QCD to next-to-leading order. The Monte Carlo generators PYTHIA and CASCADE describe the shape of the data but fall below it by factors ~ 1.8 and ~ 1.6, respectively.

References

[1] H1 Collaboration, contributed paper 5-0167 to ICHEP 2004, Peking.

[2] C. Adloff *et al.* [H1 Collaboration], Phys. Lett. B **467** (1999) 156 [Erratum-ibid. B **518** (2001) 331] [hep-ex/9909029].

[3] J. Breitweg *et al.* [ZEUS Collaboration], Eur. Phys. J. C **18** (2001) 625 [hep-ex/0011081].

[4] S. Chekanov *et al.* [ZEUS Collaboration], DESY-03-212, submitted to Physical Review D

[5] S. Chekanov *et al.* [ZEUS Collaboration], DESY-04-070 (May 2004), submitted to Physics Letters B

[6] H1 Collaboration, contributed paper 5-0164 to ICHEP 2004, Peking.

[7] H1 Collaboration, contributed paper 5-0165 to ICHEP 2004, Peking.

[8] I. Abt *et al.* [H1 Collaboration], Nucl. Instrum. Meth. A **386** (1997) 310 and 348.

[9] D. Pitzl *et al.*, Nucl. Instrum. Meth. A **454**, 334 (2000) [hep-ex/0002044].

[10] T. Nicholls *et al.* [H1 SPACAL Group Collaboration], Nucl. Instrum. Meth. A **374** (1996) 149.

[11] F. Jacquet, A. Blondel, in: Proc. *Study of an ep Facility for Europe* (Ed. U. Amaldi), DESY 79/48, p 391 (1979).

[12] S. Catani, Yu. Dokshitzer, M.H.Seymour and B.R. Webber, Nucl. Phys. B 406 (1993) 187.

[13] T. Sjostrand, Comput. Phys. Commun. **82** (1994) 74.

[14] L. Lai *et al.* [hep-ph/9903282].

[15] M. Glück, E. Reya and A. Vogt, Phys. Rev.D45, 3986(1992); Phys. Rev. D46, 1973 (1992).

[16] C. Peterson, D. Schlatter, I. Schmitt, and P.M. Zerwas, Phys. Rev. D 27 (1983) 105.

[17] S. Frixione, M. L. Mangano, P. Nason and G. Ridolfi, Phys. Lett. B **348** (1995) 633 [hep-ph/9412348].

[18] A.D. Martin, R.G. Roberts and W.J. Stirling, Phys.Lett. B354, 155 (1995); A.D. Martin, R.G. Roberts, W.J. Stirling and R.S. Thorne, Eur. Phys. J. C4 (1998) 463.

[19] D. Buskulic *et al.* [ALEPH Collaboration], Phys. Lett. B **313** (1993) 535.

[20] R. J. Barlow and C. Beeston, Comput. Phys. Commun. **77** (1993) 219.

[21] http://root.cern.ch/root/html/TFractionFitter.h

[22] H. Jung and G. P. Salam, Eur. Phys. J. C **19** (2001) 351 [hep-ph/0012143];
H. Jung, Comput. Phys. Commun. **143** (2002) 100 [hep-ph/0109102].

[23] M. Ciafaloni, Nucl. Phys. B **296** (1988) 49;
S. Catani, F. Fiorani and G. Marchesini,
Phys. Lett. B **234** (1990) 339, Nucl. Phys. B **336** (1990) 18;
G. Marchesini, Nucl. Phys. B **445** (1995) 49.

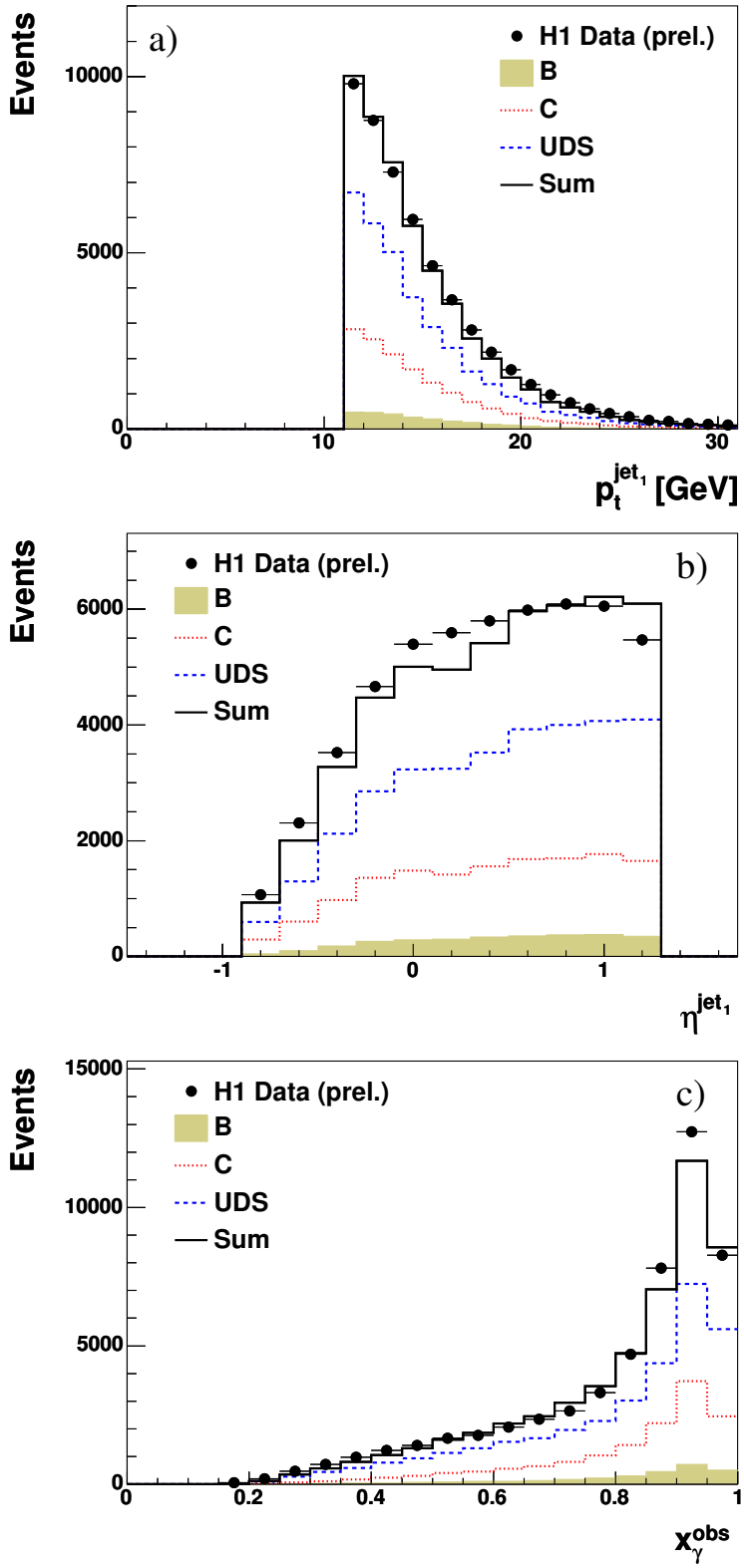

Figure 1: Distributions of the two leading jets in the final sample. a) $p_t^{jet_1}$, b) η^{jet_1}, c) x_γ^{obs}. The data (points) are compared with the PYTHIA simulation after applying the scale factors obtained from the fit to the subtracted significance distributions.

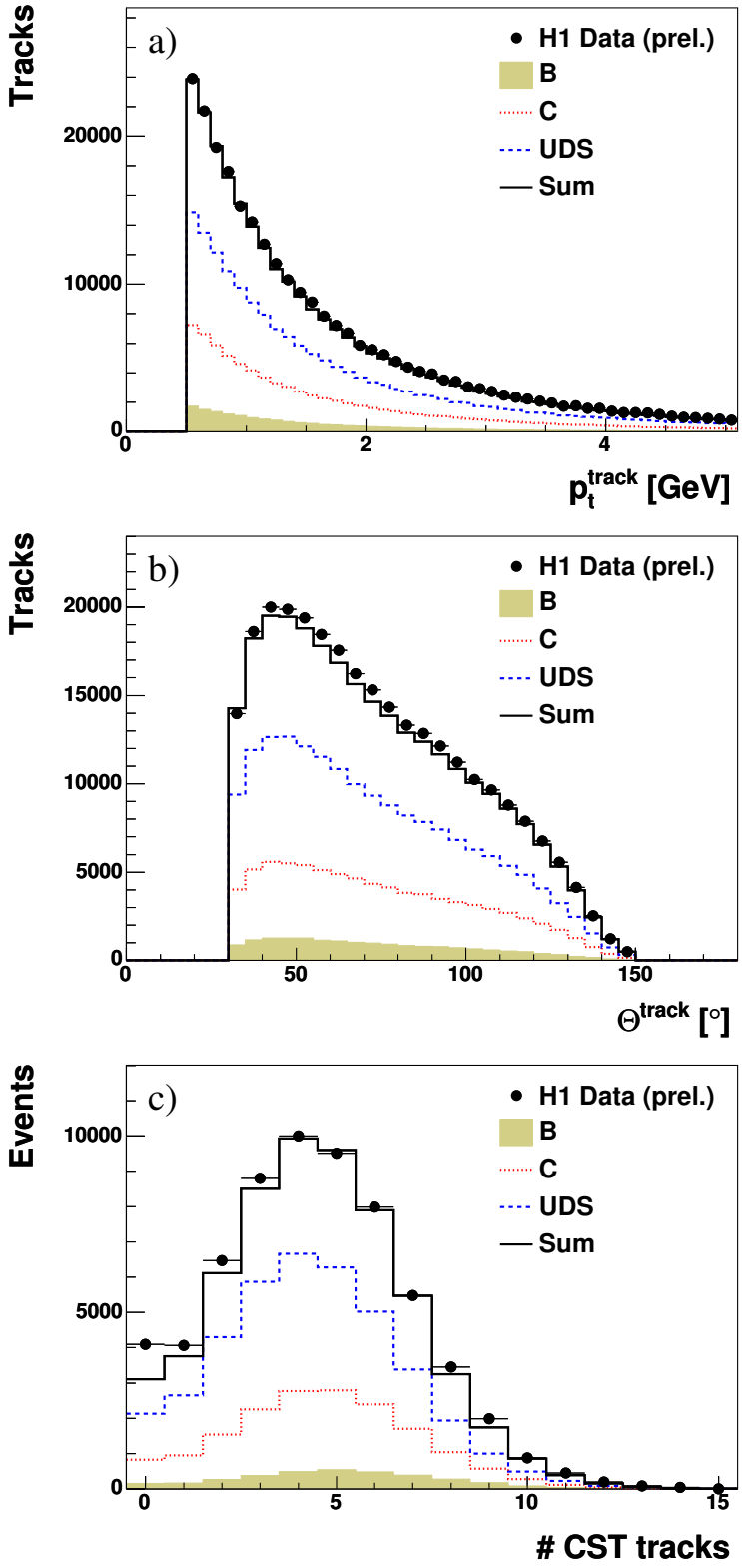

Figure 2: Distributions of the CST tracks passing the track selection requirements. a) p_t, b) θ, c) number of CST tracks. The data (points) are compared with the PYTHIA simulation after applying the scale factors obtained from the fit to the subtracted significance distributions.

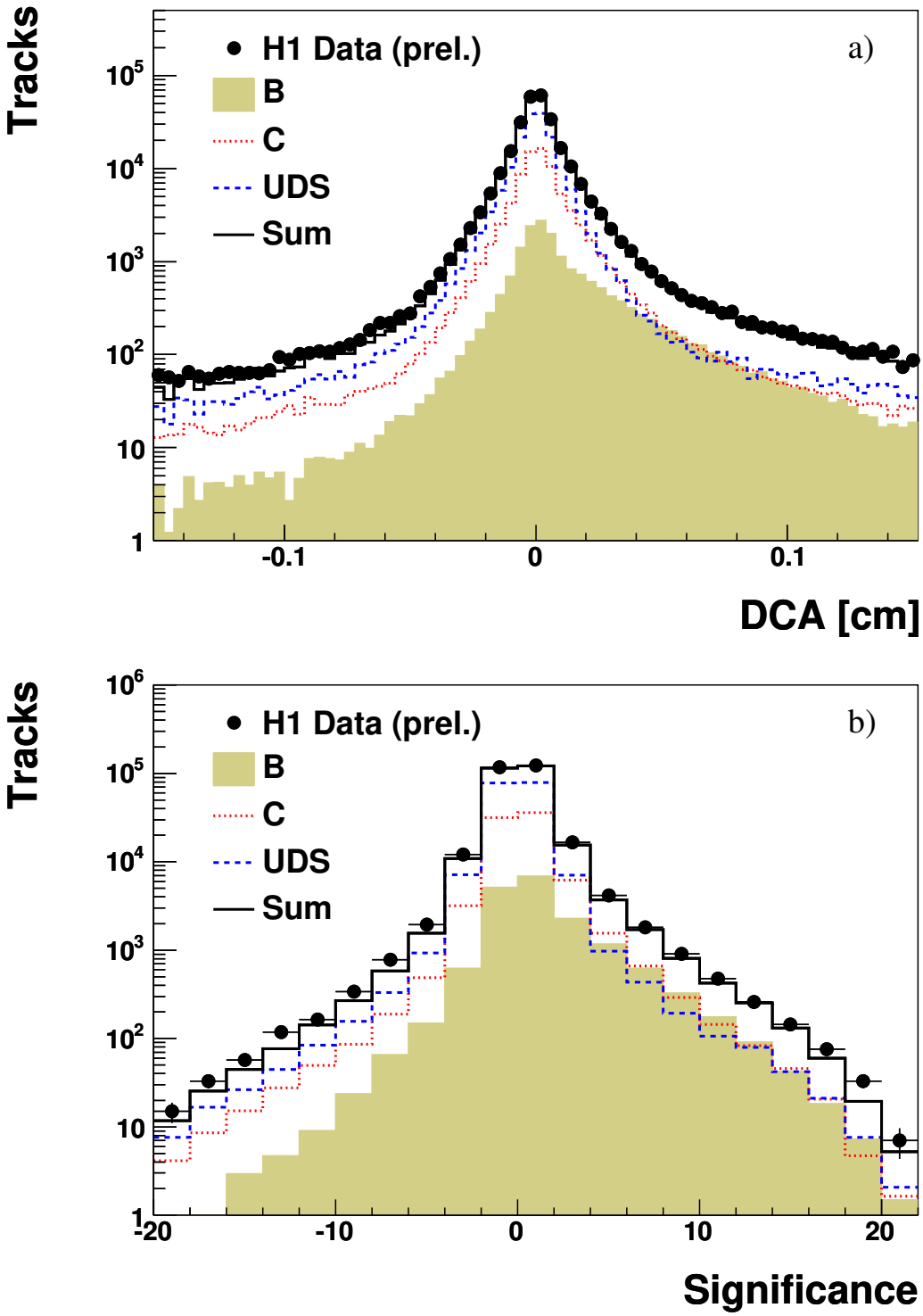

Figure 3: a) Distribution of the signed impact parameter of the selected CST tracks. b) Signed significance distribution after selection of tracks with impact parameter $|DCA| < 0.1$ cm. The data (points) are compared with the PYTHIA simulation after applying the scale factors obtained from the fit to the subtracted significance distributions.

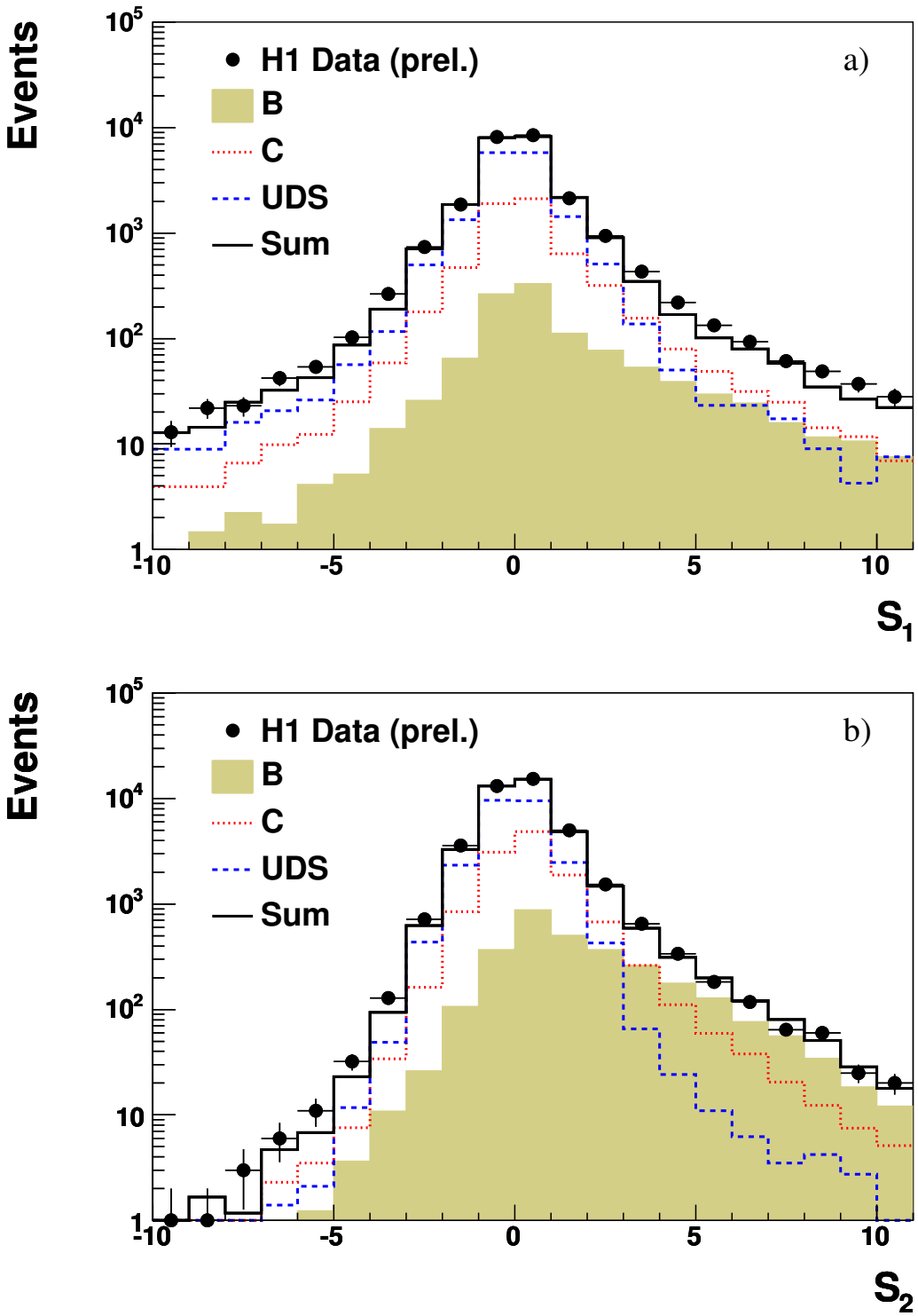

Figure 4: Significance distributions using the b, c and uds-fractions from the fit to the subtracted significance distributions of the data. a) S_1 of CST tracks in jets with exactly one CST track, b) S_2 of CST tracks with the second highest significance in jets with two or more CST tracks.

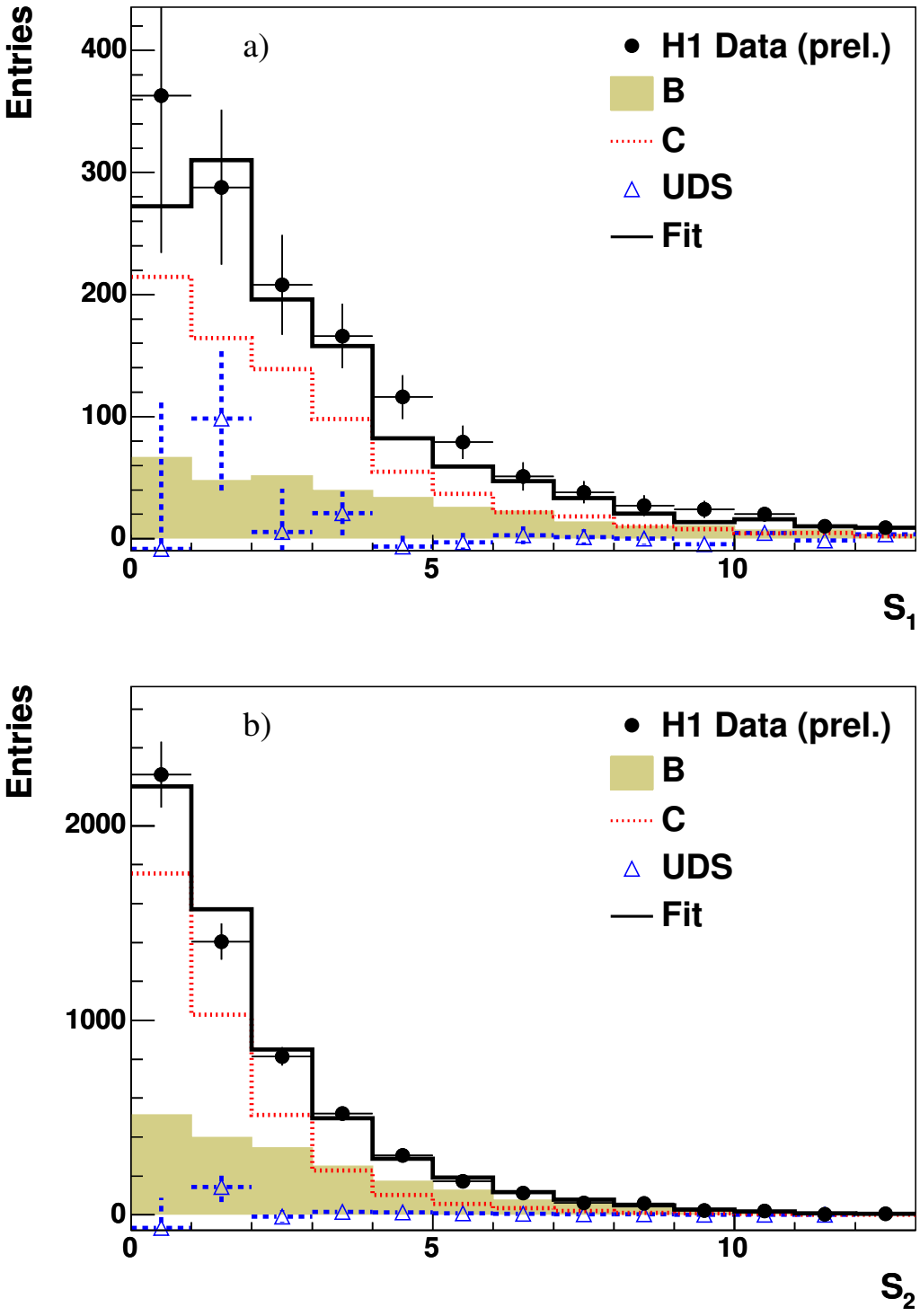

Figure 5: a) Distribution S_1 of the subtracted signed significance for the 1-track sample. b) Distribution S_2 of the subtracted signed significance for the 2- or more track sample. The data (points) are well described by the PYTHIA simulation (solid line). The decomposition of the simulation into b (shaded histogram), c (dotted line), uds (triangles) is taken from the fit as described in section 6.

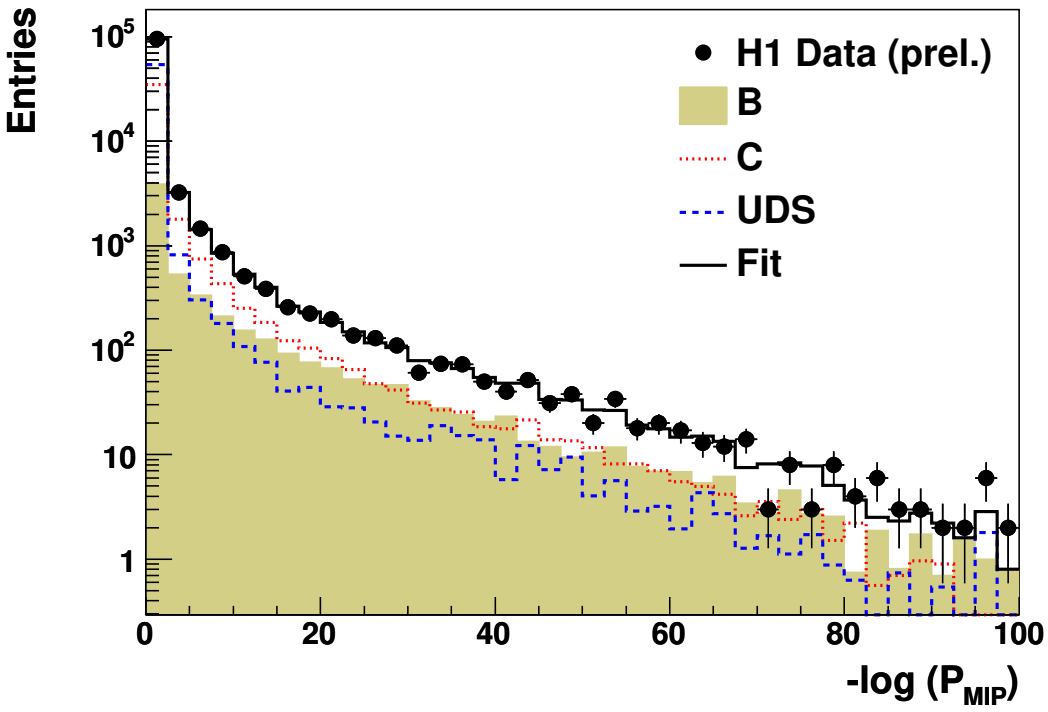

Figure 6: Distribution of the negative logarithm of the multi impact parameter probability. The decomposition of the simulation into b (shaded histogram), c (dotted line), uds (dashed line) is taken from the fit as described in section 7.

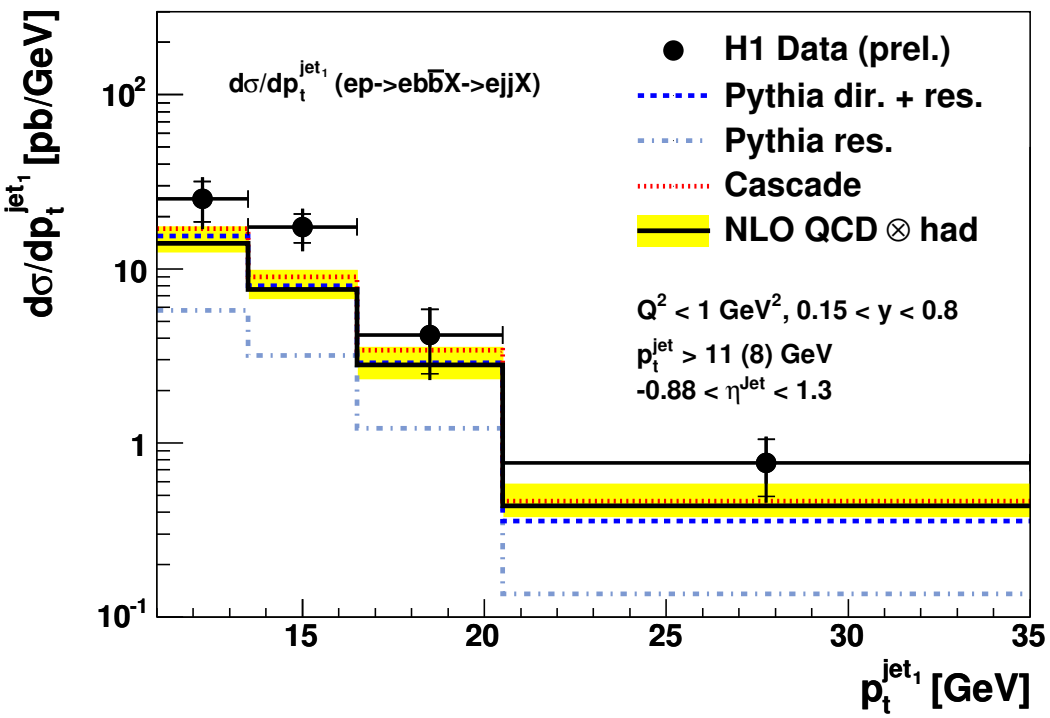

Figure 7: Differential beauty cross section $d\sigma/dp_t^{jet_1}(ep \to eb\bar{b}X \to ejjX)$ as a function of the transverse momentum $p_t^{jet_1}$ of the leading jet. The inner error bars indicate the statistical uncertainty and the outer error bars show the statistical and systematic error added in quadrature. Also shown is the prediction from CASCADE (dotted line) and PYTHIA (dashed line). The contribution in PYTHIA from processes in which the photon is resolved is shown separately (dashed-dotted line). The solid line indicates the prediction from a NLO QCD calculation and the shaded band describes the scale uncertainty of the calculation.

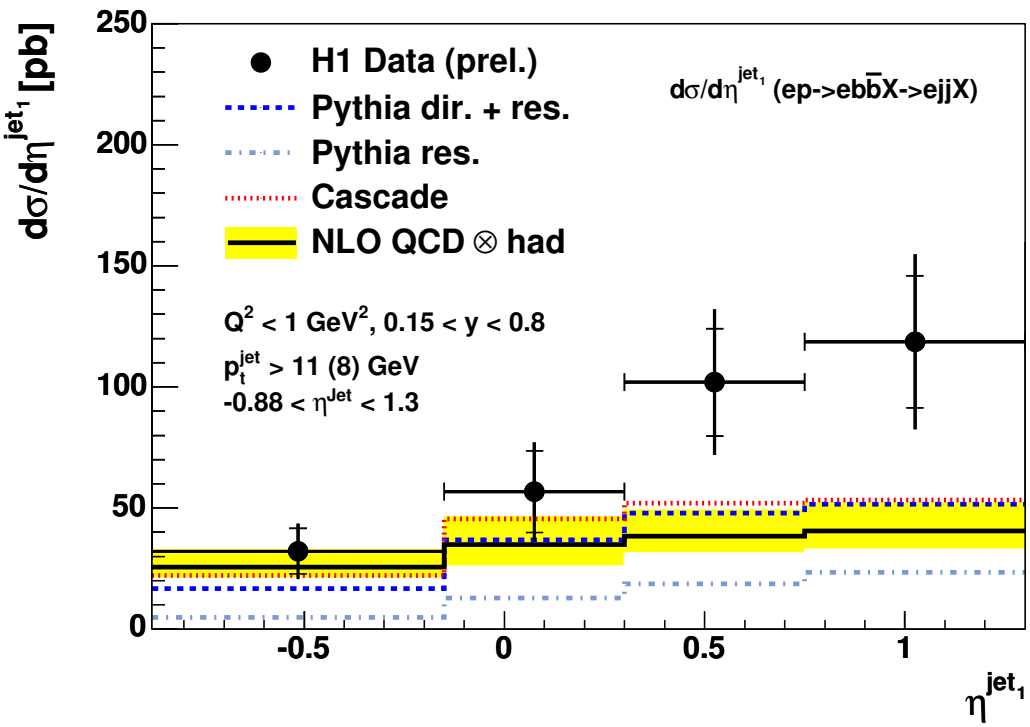

Figure 8: Differential beauty cross section $d\sigma/d\eta^{jet_1}(ep \to eb\bar{b}X \to ejjX)$ as a function of the rapidity η^{jet_1} of the leading jet. The inner error bars indicate the statistical uncertainty and the outer error bars show the statistical and systematic error added in quadrature. Also shown is the prediction from CASCADE (dotted line) and PYTHIA (dashed line). The contribution in PYTHIA from processes in which the photon is resolved is shown separately (dashed-dotted line). The solid line indicates the prediction from a NLO QCD calculation and the shaded band describes the scale uncertainty of the calculation.

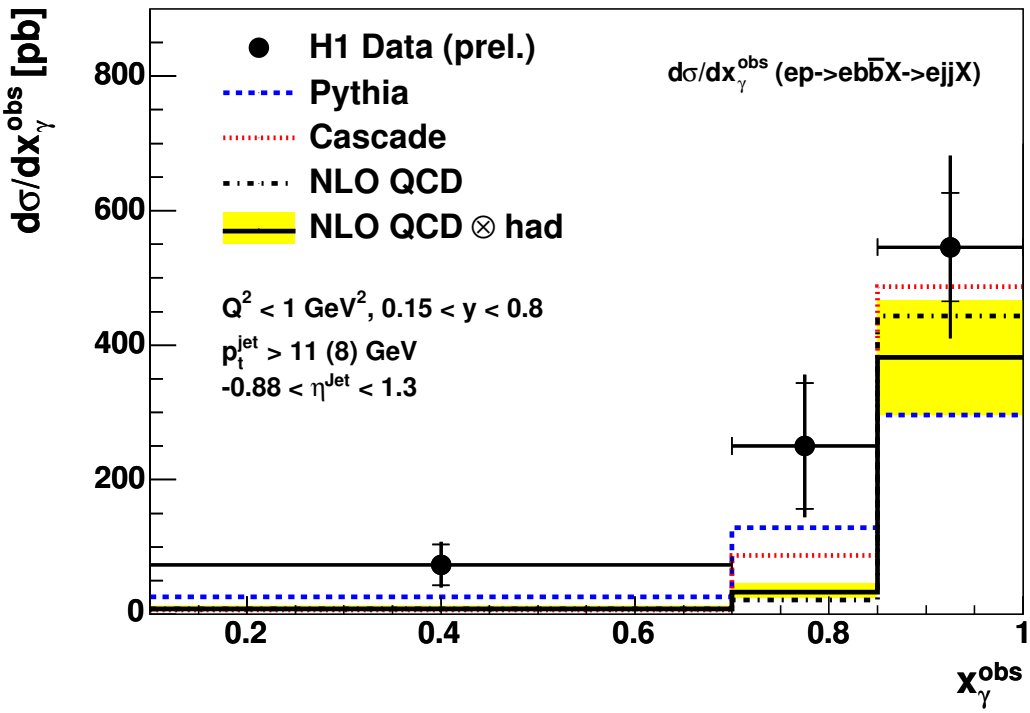

Figure 9: Differential beauty cross section $d\sigma/dx_\gamma^{obs}(ep \to eb\bar{b}X \to ejjX)$ as a function of x_γ^{obs} . The inner error bars indicate the statistical uncertainty and the outer error bars show the statistical and systematic error added in quadrature. Also shown is the prediction from CASCADE (dotted line) and PYTHIA (dashed line). The prediction from a NLO QCD calculation is shown before (dashed-dotted line) and after (solid line) hadronisation corrections, and the shaded band describes the scale uncertainty of the calculation.